

Virtual Screening with Flexible Docking and COMBINE-Based Models. Application to a Series of Factor Xa Inhibitors

Marta Murcia[†] and Angel R. Ortiz^{*,†,‡}

Department of Physiology & Biophysics, Mount Sinai School of Medicine, New York University, One Gustave Levy Place, Box 1218, New York, New York 10029, and Bioinformatics Unit, Centro de Biología Molecular "Severo Ochoa", Universidad Autónoma de Madrid, Cantoblanco, 28049 Madrid, Spain

Received March 26, 2003

A two-step, fully automatic virtual screening procedure consisting of flexible docking followed by activity prediction by COMparative BINDing Energy (COMBINE) analysis is presented. This novel approach has been successfully applied, as an example with medicinal chemistry interest, to a recently reported series of 133 factor Xa (fXa)¹ inhibitors whose activities encompass 4 orders of magnitude. The docking algorithm is linked to the COMBINE analysis program and used to derive independent regression models of the 133 inhibitors docked within three different fXa structures (PDB entries 1fjs, 1f0r, and 1xka), so as to explore the effect of receptor conformation on the overall results. Reliable docking conformations and predictive regression models requiring eight latent variables could be derived for two of the fXa structures, with the best model achieving a Q^2 of 0.63 and a standard deviation of errors of prediction (SDEP) of 0.51 (leave-one-out). The two-step procedure was then employed to screen a designed virtual library of 112 ligands, containing both active and inactive compounds. While docking energies alone could show a good performance for selecting hits, including structurally diverse ones, inclusion of COMBINE analysis regression models provided improved rankings for the identification of structurally related molecules in external sets. In our best case, a recognition rate of ~80% of known binders at ~15% false positives rate was achieved, corresponding to an enrichment factor of ~450% over random.

Introduction

Structural information about the ligand–receptor complex is becoming increasingly important in ligand optimization,^{2–4} and with the advent of the human genome and the ongoing Structural Genomics Initiatives,⁵ a large number of new pharmacological targets and their corresponding experimental or modeled structures is expected to emerge.⁶ Methods to efficiently integrate this rapidly increasing wealth of structural data with more traditional lead optimization techniques are beginning to be required in many drug discovery projects.⁷ Docking programs are being used in conjunction with large three-dimensional (3D) databases of small molecules, and different scoring functions are being designed to predict de novo ligand affinity.^{8–11} While useful in the initial stages of lead detection, available experience also indicates that predicted differences of an order of magnitude between different designs should not be relied upon as a basis for preferring one design to another. Therefore, regression-based models must ultimately be considered during the course of a drug design project so as to improve affinities. In this setting, a sufficiently rapid, automatic, and predictive QSAR-based analysis incorporating structural data of the ligand–receptor complex could become most valuable, by allowing maximal utilization of the available information in the iterative design–synthesis–test cycles.

Here we report a novel, two-step fully automatic procedure for the affinity optimization of a congeneric series against a given target of known structure. The approach is based on the use of a flexible docking algorithm followed up by structure–activity model derivation by COMparative BINDing Energy (COMBINE) analysis.^{12,13} For the first step we describe a new in-house flexible docking algorithm (see Methods for details), which differs from most other approaches in that it performs an exhaustive search of conformational space. Since the subsequent structure–activity derivation is obtained from an analysis of the interaction energetics, we considered it important to obtain complex geometries corresponding to global minima of the energy function employed (for our search space and at a given degree of discretization), even if this goal entails an increase in the computational demands. We also considered crucial, for optimal robustness and prediction ability, to have a self-consistent method that employs the well-established and widely used AMBER molecular mechanics energy function¹⁴ for both the docking simulation and the subsequent derivation of the regression model. These reasons prompted us to develop a new docking algorithm, consisting in a new alignment tool playing the same logical role of the alignment algorithms now available for CoMFA. It is not our intention to describe here a general-purpose docking algorithm. For the second part of the protocol, we derived a system-specific, receptor-based QSAR model with the COMBINE analysis methodology,¹² which allowed us to estimate binding free energy differences based on the computed interaction energies between ligand and

* Corresponding author. Phone: (34) 91-348-2376. Fax: (34) 397-4799. E-mail: aro@cbm.uam.es.

[†] Mount Sinai School of Medicine.

[‡] Universidad Autónoma de Madrid.

receptor. The COMBINE analysis method has previously proved successful for deriving high quality receptor-based QSAR models in a variety of protein–ligand complexes, including enzyme–inhibitor,^{15–19} enzyme–substrate,^{20–22} protein–DNA,²³ and peptide–protein complexes.²⁴ Since the energetics of the binding process are incorporated with modest computational requirements and the descriptors used to build the model are physicochemically sound, an advantage of COMBINE analysis is that it can potentially be applied to large datasets and to the screening of virtual libraries while preserving high predictive abilities. Despite these potential benefits, however, to the best of our knowledge the applicability of COMBINE analysis to virtual screening has not previously reported in the literature, and this constitutes the first successful example.

As a test case we chose a recently reported congeneric series of factor Xa (fXa) inhibitors.¹ This series was chosen not only because of its desirable properties (see Methods) regarding number of compounds, diversity, and affinity range, but also for their interest from a medicinal chemistry standpoint. fXa is a member of the trypsin-like family of serine proteases, an important family of pharmacological targets relevant to a number of diseases.^{25,26} In particular, fXa plays a critical role in the formation of blood clots by ultimately regulating the proteolysis of prothrombin to thrombin, the first step that links the intrinsic and extrinsic coagulation pathways for converging to a final common route.²⁷ This key location, together with its role in thrombin activation and potentiating effects on clot formation, identify it as an attractive target in anticoagulant/antithrombic drug development.^{28,29} The fXa inhibitors analyzed in this paper correspond to a series of 138 compounds, originally described by Matter and co-workers and used by these authors for the derivation of successful 3D-QSAR models.¹

The paper is organized as follows: first, in the Methods section we describe the docking algorithm and the COMBINE analysis method. Then, in the Results and Discussion sections, we describe the accuracy of the docking method, the predictive ability of the complex-based regression models, and the performance of the two-step approach in virtual screening experiments of molecular datasets. This is compared with the use of the *naked* AMBER energy function¹⁴ employed within the docking program. Finally, we close this paper with a summary of the main conclusions obtained in this work.

Methods

Docking Algorithm. Energy Function. The non-bonded interaction energies of the AMBER force field¹⁴ (parm.99 parameter set³⁰) using an all-atom model were employed to model the ligand–receptor interaction. The equation used here has the following form:

$$E_{\text{MM}} = \sum_i \sum_j^{\text{prot lig}} \left[\frac{A_{ij}}{r_{ij}^{12}} - \frac{B_{ij}}{r_{ij}^6} + 332 \frac{q_i q_j}{\epsilon r_{ij}} \right] \quad (1)$$

A_{ij} and B_{ij} represent the van der Waals (VDW) parameters of the atom types assigned to atoms i and j . $A_{ij} = \epsilon_{ij} r_m^{12}$ whereas $B_{ij} = 2\epsilon_{ij} r_m^6$. Parameters ϵ_{ij} (in kcal/mol) and r_m (in Å) are obtained by applying the

Lorentz–Berthelot mixing rules. On the other hand, q_i and q_j are the partial charges of atoms i and j , respectively, and r_{ij} (in Å) is the distance between them.³¹ We refer to the AMBER potential for details about parameters.¹⁴ Hydrogen and oxygen radii were scaled down with a factor of 0.8 for optimal performance, based on trial and error tests (test results not shown). A distance-dependent dielectric constant, $\epsilon = 4$, was used. We have made some tests with more complicated electrostatic models, but we did not observe in any of the cases a statistically significant improvement in the docking success rate (data not shown).

Automatic Ligand Parametrization. Ligand parametrization is automatically generated by means of an analysis of the molecular topology of the ligand using graph theory. After building the connectivity matrix of the ligand, a depth-first search through the nodes of the resulting graph is conducted. This allows the detection and storage of bonded atoms, 1–4 atom groups, rings, and fused rings in the molecule, as well as the location of heteroatoms relative to the rings and the definition of atomic hybridization states, among various topological data. Once this information is gathered, the algorithm attempts, in a second step, to assign AMBER atom types¹⁴ to the molecule. This is done based on a library of atom types and a set of classification rules that use the topological data previously stored. At the time of this writing, 22 different atom types from the parm.99 parameter set³⁰ of the AMBER force field¹⁴ are being used and assigned (see Table A1, Supporting Information, for atom types and rules). Atoms not falling into any of the categories used by the program are assigned generic types. Separately, unscaled atom-centered charges for the ligand are obtained³² from a linear fitting to the molecular electrostatic potential computed using the AM1 Hamiltonian³³ with the MO-PAC program.^{34,35}

Ligand Conformational Search. A torsion-driven algorithm was developed to search the ligand conformational space. Only torsion angles in rotatable bonds are considered, with a rotatable bond defined as a single or exocyclic double bond having at least one non-hydrogen neighbor on each side of the bond. Rotations affecting oxygen atoms in terminal groups, such as carboxylates, phosphates, sulfonyl, etc., are skipped. Amide bonds are not scanned unless asymmetric substitution is present on the amide nitrogen; otherwise a 180° angle value is fixed for the dihedral X–N–C–X. Sulfoamino nitrogen atoms are treated with sp³ hybridization. If a dihedral angle X–S–N–X needs to be scanned, alternative eclipsed conformations (0°, 120°, –120°) are considered. Only rotameric states are considered in general (although there are some special cases; see below), with the following dihedral angles: 60°, 180°, and –60° for sp³–sp³ bonds; 0°, 60°, 120°, 180°, –60°, and –120° for sp³–sp² bonds (when symmetry is present on sp² only 60°, 180°, and –60° are considered to avoid redundancies); and 0°, 180° for sp²–sp² bonds (again, symmetry existence is checked). There are a few special cases: for sp²–sp² rotatable bonds attached to aromatic systems 0°, 90°, 180°, –90° angles are used (when symmetry is present on sp² only 0°, and 90° are scanned to avoid redundancies); on the other hand oxygen–sp³ bonds in esters and ethers are treated

as regular sp^3-sp^3 bonds except in cases where the sp^3 center is located in a ring (e.g. ribose, glucose derivatives), where eclipsed conformations are a common trend. For these we consider 0° , 60° , 120° , 180° , -60° , and -120° .

All possible dihedral angle combinations are generated, and the corresponding intramolecular energy of each of the resulting conformations is computed based on nonbonding 12–6 Lennard–Jones terms, without considering 1–2 and 1–3 interactions, and with 1–4 interactions scaled down by a factor of 2, as it is customary within the AMBER force field.¹⁴ No energy minimization is performed in any of the conformations; thus, a VDW energy cutoff of 5 kcal/mol is used to cap each pairwise interaction. Only conformations with computed VDW energies within 30 kcal/mol of the global minimum are saved for docking. To reduce the combinatorial explosion, for sp^3-sp^2 bonds the program first evaluates the local energy, up to 1–4 interactions, associated with each of its six dihedral angles. The three lowest energy values are then used in the combinatorial search. This procedure proved very successful in keeping the combinatorial size under control, while having minor effects on the rate of bioactive conformation generation and docking accuracy (data not shown).

The approach is designed specifically to have a high information/CPU ratio. It has been shown recently that the more sophisticated methods deliver only a small margin of statistical improvement in reproducing bioactive conformations with respect to the simple, rotameric-based torsional search.³⁶

Grid Description of the Binding Site. The intermolecular energy is precomputed using an underlying 3D grid. A gridded box is created by adding a 3.5 Å cushion to the maximum dimensions of the ligand complexed with the protein and using a grid spacing of 0.3 Å. Then, for a ligand atom probe j at grid point (k,l,m) , the total interaction energy with all protein atoms i is computed according to eq 1. Precalculating the contribution of every receptor atom at every grid point can be frustratingly lengthy, especially when large sampling volumes are used. For this reason, and for VDW terms only, a 12 Å cutoff around each grid point is imposed. Only protein atoms within this specified distance are considered. The precomputed grid energy is then used during docking to calculate the protein–ligand interaction energy for each conformer atom from a trilinear interpolation, using the nearest eight grid points surrounding the atom.³¹

Exhaustive Search Algorithm. A complete enumeration of all possible orientations of each ligand conformer in the active site of the rigid protein is computed. The conformer is translated and rotated in the docking region using the ligand center of mass, which is moved consecutively to every grid point in the box using a grid spacing of 0.6 Å. At each grid point, a complete sampling of the rotational space is achieved by computing all nondegenerate sets of Euler angles with a resolution of 27° .³¹ From here, the algorithm switches to a greedy search. The best 512 energy orientations obtained after this initial search with each conformer are subjected to rigid body off-lattice energy minimization using the SIMPLEX algorithm from Nelder & Mead.³⁷ The lowest energy pose obtained is stored as

the docking energy for that particular conformer. The lowest energy conformation among all energies of the conformers is taken as the predicted binding mode for the ligand.

Docking Studies. Datasets Selection and Description. We tested the performance of the flexible docking procedure by studying two different datasets. First, a general set of 55 noncovalent protein–ligand complexes selected from the Protein Data Bank PDB³⁸ (Table 1), with a broad range of diversity in both their ligand structure (including atom types, number of rotatable bonds, etc.) and binding site shapes. As a second set, a series of sialic acid and benzoic acid analogues described as inhibitors of the influenza type A neuraminidase (NA) and cocrystallized with different forms of this enzyme were used. These compounds, which have been previously studied using COMBINE analysis,¹⁹ provide a good system for testing both the direct docking as well as the cross-docking performance of our algorithm which considers only one rigid structure for the protein. Only the X-ray structures were considered: 9 N2-strain A/Tokyo/67- and 23 N9-strain A/Tern/Australia/G70c/75- subtypes (8 wild-type + 7 N9 Arg292Lys mutants + 8 Gly336Asn N9 mutants). Two more influenza type B-strain B/LEE/40- NA in complex with related ligands (PDB entries 1b9t and 1b9v) completed the selection, giving a total of 34 complexes containing 28 different inhibitors and three subtypes of NA.

Preparation of Complexes for Docking. Protein and ligand structural data were separated into different files. Water molecules were removed from the protein when present (except in NA series where the original set up conditions for the protein file, containing some water molecules, were kept as in the COMBINE analysis from which they were taken).¹⁹ Protein hydrogen atoms were first positioned using the protonate program from the AMBER 7.0 package,³⁹ while for the ligand, hydrogen atoms were added using the InsightII⁴⁰ builder module, in both cases assuming physiological conditions. As a rule, all carboxylic acid and phosphoric acid groups were ionized, while all basic amino, amidino, and guanidino groups were protonated. The orientation of rotatable OH and NH_3 groups was not optimized. Standard AMBER force field¹⁴ charges and atom types were used for the protein whereas the ligand was treated as previously described.

We emphasize that during the conformational search, the conformation of the bound ligand did not form part of the pool of conformers at any point. All conformers in the pool were generated by assigning canonical rotameric states. As initial structures for this conformational search, we used two sets: in one the bound structure of the ligand was employed to carry out this dihedral assignment. In a second set we started from structures generated from scratch using standard bond lengths and angles by applying CORINA^{41,42} with default settings. These CORINA-generated structures were then subjected to the same exact protocol for conformer generation and docking.

Docking Evaluation. As metric for the evaluation of the docking protocol, we used the root-mean-square deviation (RMSD) of the best energy-scored solution compared to the ligand position in the crystal structure.

Table 1. Performance of the Docking Algorithm. Table Sorted by Number of Torsionals in the Ligand (ntor)

PDB ID ^a	nat ^b	char ^c	ntor ^d	log rotset ^e	RMSD dock ^f	ENE dock ^g	first rank ^h	first RMSD ⁱ	gap VDW ^j	VDW/h atm ^k
1abe	20	0	0	0.0	0.25	-31.10	ND'	ND'	ND'	-1.18
1abf	23	0	0	0.0	0.40	-32.80	ND'	ND'	ND'	-1.13
1dbj	51	0	0	0.0	0.35	-42.07	ND'	ND'	ND'	-0.79
1mrg	15	0	0	0.0	0.47	-24.77	ND'	ND'	ND'	-1.21
1cbs	49	-1	1	0.6	2.12	-55.68	2	0.66	7.17	-1.69
1d3h	28	0	1	0.3	0.35	-49.40	1	0.35	19.12	-1.75
1dbb	53	0	1	0.5	1.96	-36.43	1	1.96	1.44	-1.53
1fen	50	0	1	0.6	0.59	-38.62	1	0.59	17.52	-1.93
1flr	36	-1	1	0.3	0.64	-73.37	1	0.64	-2.44	-1.33
1tng	24	1	1	0.5	0.30	-13.96	1	0.30	0.63	-2.74
1tnh	18	1	1	0.5	0.59	-15.30	1	0.59	2.07	-2.37
1tnl	22	1	1	0.5	1.85	-7.83	1	1.85	1.11	-2.10
2cbs	54	-1	1	0.6	0.40	-62.24	1	0.40	12.19	-1.59
1bju	34	1	2	0.6	1.96	-27.40	1	1.96	-0.34	-1.45
1c5c	32	-1	2	1.0	0.86	-92.09	1	0.86	8.71	-1.60
1f3d	33	1	2	1.0	0.43	-34.43	1	0.43	1.66	-2.18
1hsl	20	0	2	1.0	0.41	-54.22	1	0.41	7.26	-2.30
1mid	18	-3	2	1.0	2.05	-196.21	8	0.47	3.27	-1.37
1mrk	32	0	2	1.0	1.38	-48.04	1	1.38	-0.67	-1.76
1wap	27	0	2	1.0	0.83	-42.76	1	0.83	-0.10	-1.60
7tim	14	-2	2	1.0	1.59	-43.63	1	1.59	-0.03	-2.00
1ejn	53	1	3	1.3	1.99	-42.68	1	1.99	-4.35	-1.09
1rnt	36	-2	3	1.4	3.53	-7.71	13	1.30	-0.54	-0.91
1srj	33	-1	3	1.8	1.32	-42.01	1	1.32	1.79	-1.63
1tnk	24	1	3	1.4	2.06	-14.54	2	1.55	1.37	-2.30
2ak3	35	-2	3	1.4	3.15	-133.92	13	0.49	6.34	-1.33
1tni	27	1	4	1.8	2.64	-26.85	14	1.98	1.61	-2.18
1b9t	41	0	4	1.7	0.64	-64.48	1	0.64	-2.20	-1.38
1bjv	45	1	4	1.5	1.93	-29.50	1	1.93	3.60	-1.32
1lst	25	1	4	1.8	0.31	-115.04	1	0.31	5.52	-2.59
1snc	37	-4	4	1.8	1.23	-348.16	1	1.23	5.65	-1.36
6rnt	36	-1	4	1.8	0.54	-15.34	1	0.54	3.60	-1.25
1fpu	47	0	5	2.0	1.02	-51.26	1	1.02	2.53	-1.68
1mts	65	1	5	2.3	3.21	-33.45	NF ^m	NF ^m	-2.20	-0.99
2dbl	67	-1	5	2.0	1.76	-41.18	1	1.76	0.52	-1.31
3tpi	38	0	5	2.2	0.50	-63.98	1	0.50	7.05	-2.48
4dfr	54	-1	5	2.2	2.35	-77.30	41	1.30	1.70	-1.22
1hsb	39	1	6	2.8	1.01	-54.18	1	1.01	-0.08	-1.72
1rds	63	-1	6	2.8	0.92	3.01	1	0.92	2.18	-1.13
1rt1	44	0	6	2.2	0.57	-34.25	1	0.57	6.93	-1.55
2fox	52	-2	6	2.5	1.32	70.20	1	1.32	1.91	-1.52
1aqw	36	-1	7	3.2	3.64	-36.24	7	1.05	0.16	-1.21
1b9v	50	-1	7	2.8	0.97	-78.05	1	0.97	1.19	-1.53
1kel	39	-3	7	2.6	1.49	-222.29	1	1.49	1.31	-1.42
1ppc	69	1	7	2.8	2.08	-33.80	NF ^m	NF ^m	2.66	-1.14
1rt2	51	0	7	2.4	1.04	-41.25	1	1.04	34.60	-1.48
2tsc	56	-2	8	3.1	2.25	4.24	5	1.96	-1.08	-1.37
3ert	59	1	8	3.1	0.80	-113.95	1	0.80	1.25	-1.81
1d0l	62	-2	9	3.7	7.05	-145.39	NF ^m	NF ^m	-1.21	-0.76
1ajv	75	0	10	3.1	1.96	15.03	1	1.96	49.00	0.46
1ajx	74	0	10	3.8	0.62	-60.44	1	0.62	3.51	-1.41
1bma	73	1	10	3.7	6.85	-36.58	656	1.88	2.63	-0.84
1fkg	68	0	10	3.2	2.27	-39.44	13	1.84	1.09	-1.18
1fkh	74	0	10	3.6	1.88	-40.38	1	1.88	1.01	-1.16
1hvp	70	0	11	3.8	4.15	-50.84	93	1.78	4.15	-1.34

^a PDB ID, Protein Data Bank entry. ^b nat, total number of ligand atoms. ^c char, ligand formal charge. ^d ntor, total number of rotatable dihedral angles in the ligand. ^e logrotset, number of ligand rotamers selected for docking analysis (within 30 kcal/mol of the lowest energy) expressed in logarithmic units. ^f RMSD dock, docking RMSD (Å) of the docked (best energy scored) conformation coordinates compared with the crystal structure; a docking RMSD of 2.0 Å or less is considered a successful solution. ^g ENE dock, computed docking energy (kcal/mol). ^h first rank, first docking solution with RMSD equal or less than 2.0 Å according to an energy-based rank. ⁱ first RMSD, RMSD of the first rank. ^j gapVDW, energy difference (kcal/mol) between the VDW energy of the best scored docking solution and the VDW docking energy average corresponding to the five following solutions in the energy ranked list of docked conformations. ^k VDW/h atm, average VDW docking energy per ligand heavy atom (kcal/mol). ^l ND, not determined. For ligands without rotatable bonds (ntor = 0), only one docking solution corresponding to the rigid docking of the unique conformation is saved. ^m NF, not found. Shaded entries correspond to program failures in finding the correct binding mode as the lowest energy pose (RMSD greater than 2.0 Å).

In keeping with standard practices in the docking field,⁹ we considered that a correct binding mode has been reproduced when RMSD between predicted and experimental coordinates was less than or equal to 2 Å. Direct RMSD calculations used standard algorithms, considering heavy atoms and atom equivalences. For cross-docking, pairwise superimposition with the MAMMOTH⁴³ program was employed to obtain the alignment between the protein considered for docking and the actual binding partner of the ligand in the PDB. The rotation matrix and translation vector obtained in this way were applied to the ligand coordinates prior to the RMSD computation.

COMBINE Analysis Theory Overview. For the sake of completeness, we briefly summarize the basis of the COMBINE analysis here.^{12,13} In COMBINE, the binding free energy ΔG of the receptor–ligand complex (or an equivalent expression such as pK_i , pIC_{50} , etc.) is correlated with a set of selected interaction energy

components. Each selected energy component u_i contributes to the binding free energy according to its weight w_i :

$$\Delta G = \sum w_i u_i + C \quad (2)$$

Having a sufficiently high number of molecules with known affinity in a training set and a dataset of ligand–receptor models for these molecules, we can estimate weights by linear fitting.

Since in the linear system in eq 2 there are usually many more unknowns than equations, the use of standard multiple regression techniques is precluded, but a solution can be found by applying partial least squares (PLS) analysis. Details of the PLS algorithm are outside of the scope of this paper, but excellent references are available.⁴⁴

The energy terms entering eq 2 should reflect as

closely as possible a true partition of the binding free energy. Entropic terms are however elusive to incorporate, so that it is customary to introduce only electrostatic interactions, u_i^{ele} , and VDW interactions, u_i^{vdw} , between the inhibitor and each protein residue in the energy-minimized structure to estimate the pK_i value:

$$pK_i = \sum_i w_i^{\text{vdw}} u_i^{\text{vdw}} + \sum_i w_i^{\text{ele}} u_i^{\text{ele}} + C \quad (3)$$

The important residues contributing to the activity should exhibit large w_i^{vdw} and/or w_i^{ele} values. Note that a larger (more positive) pK_i value in eq 3 represents stronger binding and corresponds to a more negative binding free energy, ΔG , in eq 2.

The major advantages of this procedure over simply correlating the observed ΔG with the total computed binding energy are (i) that errors either in the field parametrization or in modeled 3D structures can be, at least partly, filtered out by the PLS analysis, and (ii) that the resultant model can help to pinpoint those interactions that are key for the observed differences in binding affinity. This latter information can provide important hints both for the design of molecules with improved binding properties and for the prediction of point mutation effects. The basis of this paper is to show that these analyses can be automated to screen ligand libraries.

COMBINE Analysis of FXa Inhibitors. A series of 3-amidino-1*H*-indole-2-carboxamides and analogues as inhibitors of fXa¹ was used as an application of the methodology. The general chemical scaffold and structural variations in the series are schematically shown in Figure 3. All compounds reported in the original study were used, with the exception of racemic compounds, resulting in a set of 133 compounds out of the 138 initially described, with inhibitory activities covering 4 logarithmic units.¹

Protein–Ligand Docking. Molecules were modeled in InsightII⁴⁰ Builder module in arbitrary conformations, using standard bond lengths and angles. The benzamidine moiety and basic amino functional groups were protonated, and amides and primary and secondary amino groups adjacent to aromatic portions were treated as uncharged. All carboxylate groups were considered to be deprotonated. Atomic charge calculations and conformational sampling were carried out as described before. Three publicly available X-ray structures of fXa in complex with nonpeptidic benzamidine-related inhibitors (PDB entries 1fjs,⁴⁵ 1f0r,⁴⁶ and 1xka⁴⁷) were selected for the docking studies and COMBINE analysis of the indole derivatives. The previously described docking protocol was used for each of these receptor templates, and the rest of the procedure was carried out in parallel for each of the three sets of fXa–inhibitor complexes.

Energy Minimization of the Complexes. In preparation for COMBINE analysis, topology and coordinate files of each modeled complex were obtained with the tLEaP module from AMBER 7.0,³⁹ and their geometries were refined with module sander following an energy minimization protocol consisting of 100 steps of steepest descent and up to 400 steps of conjugate gradient during which only protein atoms were allowed to relax. A distance-dependent dielectric constant, $\epsilon = 4r_{ij}$, was

Table 2. COMBINE Analysis Performance for the fXa Inhibitors Series^a

PDB ID	1fjs	1f0r
number of variables	286*2	286*2
number of LV	8	8
<i>n</i>	114	107
R^2 (fitting)	0.752	0.761
SDEC	0.415	0.394
Q^2 (cross-validation)	0.628	0.607
SDEP	0.509	0.506

^a Abbreviations: PDB ID, Protein Data Bank entry used for generating the fXa–inhibitor complex models; LV, latent variables; *n*, number of compounds in the training set; R^2 , correlation coefficient (fitting performance given by $R^2 = 1 - [\sum_{i=1}^n (y_{\text{exp}(i)} - y_{\text{fitt}(i)})^2] / [\sum_{i=1}^n (y_{\text{exp}(i)} - \langle y_{\text{exp}} \rangle)^2]$ where $y_{\text{fitt}(i)}$ corresponds to the value of the quantity fitted with the model for complex *i*, $y_{\text{exp}(i)}$ is the experimental value of the quantity for complex *i*, and $\langle y_{\text{exp}} \rangle$ is the average experimental value of the quantity for the complete set of *n* complexes); Q^2 , predictive correlation coefficient (the equivalent of R^2 calculated for the cross-validated predictive performance); SDEC, standard deviation of errors of correlation (given by $\text{SDEC} = \{[\sum_{i=1}^n (y_{\text{exp}(i)} - y_{\text{fitt}(i)})^2] / n\}^{1/2}$); SDEP, standard deviation of errors of cross-validated prediction (the equivalent of SDEC calculated for cross-validation).

used throughout, and no cutoff distance was used in the evaluation of nonbonded interactions. We note that, since the conformation of the ligand was kept frozen, no intramolecular ligand force field terms were required during the minimization, facilitating the high-throughput character and automation of the approach.

Chemometric Analysis. All computations were carried out with our in-house program COMBINE. For comparison purposes and easier manipulation, only common residues within the three fXa structures were considered, yielding a total of 286 residues, the number present in the 1f0r PDB entry.⁴⁶ Therefore, each complex was then described by 286 intermolecular electrostatic energy variables (using a dielectric constant of $\epsilon = 4$) and 286 intermolecular VDW energy variables, giving a total of 572 unscaled *x*-variables which were used directly in the analysis without further pretreatment. Introduction of additional external variables, such as electrostatic desolvation energies, entropy estimations, or distance-dependent dielectric constants, did not produce improved models (data not shown). The *y*-variable was assigned as pK_i . Initial PLS analysis with the 133 complexes gave leave-one-out (LOO) cross-validation Q^2 values in the range of 0.3, due to the presence of some outliers. We ascribed the existence of these outliers to wrong docking modes predicted by our docking program (vide infra, Results and Discussion). These complexes were removed, and PLS analyses were repeated. This procedure gave final training sets of 114 (1fjs), 107 (1f0r), and 113 (1xka) compounds. Statistics from the analysis of the 1fjs- and 1f0r-based models are found in Table 2 and are further discussed in the Results and Discussion sections, while the poorer quality of the final 1xka-based regression model made us discard it for further applications.

Since we removed some of the complexes from the set, it was important to establish the robustness of the generated regression models. Two tests were carried out. The first was a scrambling test: activity data for each final COMBINE analysis training set (1fjs and 1f0r-based models) were randomly scrambled 100 times, producing 100 regression models with the randomly assigned activities, which were further analyzed and are

described in the Results section. For the second test, external cross-validation was simulated by randomly taking 13 complexes from the *original dataset* of 133 compounds and using them as external sets, while the remaining complexes were used to derive COMBINE analysis models, exactly in the same way as described above. Twenty such test models were generated for the 1fjs and 1f0r sets of complexes, and these are discussed in the Results and Discussion sections.

Virtual Screening Experiments. We have investigated the use of the two-step procedure, flexible docking, and external pK_i prediction with COMBINE, to automatically screen virtual libraries. For this purpose, we have designed a small in-house virtual library of 99 ligands, containing both inactive and active compounds (see Tables A2 and A3, Supporting Information). Ligands were prepared and docked into the fXa binding site (using both 1fjs and 1f0r PDB entries) as previously described. In our evaluation protocol, 20 different sets of molecules (each containing 13 randomly chosen compounds) were left-out, one at a time, from the original list of 133 inhibitors and mixed with the rest of the compounds (see Tables A2 and A3, Supporting Information) that made up the virtual library. Thus, each trial of the library consisted of 86 inactive molecules (Table A2, Supporting Information), although we do not have experimental data to support this contention, 13 fXa inhibitors not related to the series (Table A3, Supporting Information), and 13 inhibitors from the Matter et al. series not used in the derivation of the COMBINE analysis model. Each COMBINE analysis model derived for the remaining 120 fXa ligands was then used to screen the library.

The screening results were analyzed using the familiar Receiver Operating Characteristic (ROC) plots:⁴⁸ the 13 known fXa inhibitors that were not members of the series studied were marked as active, a pK_i cutoff of 5.5 was used to regard the 13 excluded series members as active or inactive, and the remaining 86 compounds in the library were marked as inactive. The active/inactive list was ranked according to the COMBINE analysis predicted affinity. The percentage of successfully found binders (true positives) was scanned through the ranked database and plotted as a function of the cumulative percentage of nonbinders (false positives) (Figure 8). In addition, enrichment factors⁹ (concentration of binders in a subset/concentration of binders in the database) were also computed through the database and plotted against the corresponding percentage of the screened database (Figure 9).

For comparison, the screening methodology was also pursued for both sets of complexes (1fjs and 1f0r) using the *naked* AMBER energy function employed within our docking program. Ligand sets were ranked according to their computed docking energy, and ROC and enrichment factor plots were then produced as described before (Figures 8 and 9). Average plots are presented except for the docking energy-based virtual search of fXa inhibitors that were different from the studied series, where only one list results.

Results

Evaluation of the Docking Algorithm. We have tested the performance of the flexible docking procedure

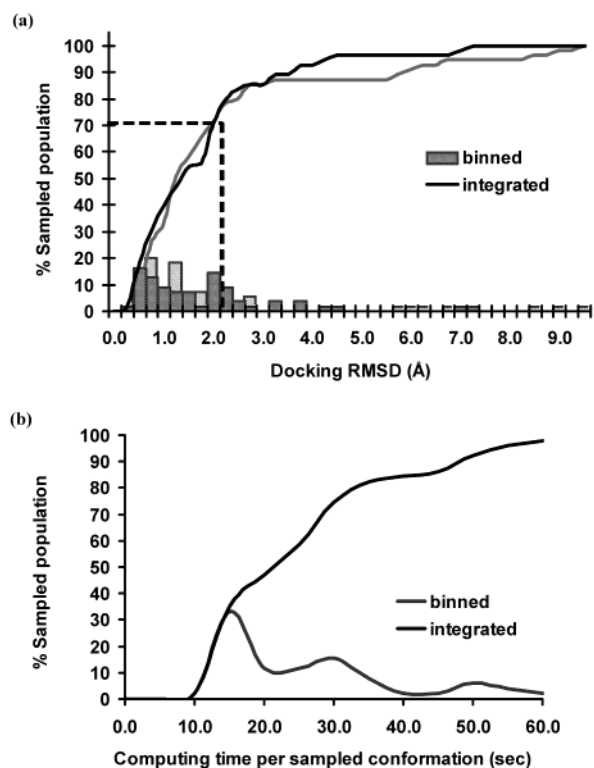


Figure 1. Histograms showing (a) the docking RMSD (Å) distribution starting either from the crystallographic ligand structure (darker line and bars) or from de novo built ligand structure (lighter colors) when generating the rotamers to be docked (see text for details) (RMSD of 2.0 Å or less is considered a successful solution) and (b) the computing time (sec) distribution in our docking validation set of 55 complexes. In all cases, both binned and integrated distributions are shown.

by assessing its ability to reproduce the experimental docking orientation, as expressed in terms of the RMSD of the lowest energy pose found by the program. We studied two different test sets, a first series of 55 structurally diverse complexes, and a second series of 34 NA inhibitors that have been cocrystallized with different forms of this enzyme.¹⁹

Docking Performance with the General Test Set. The performance of the docking algorithm on the set of 55 structurally diverse protein–ligand complexes is shown in Table 1. The results are summarized in Figure 1, which displays the binned and integrated RMSD distributions for the lowest energy poses in the test set. In 40 out of 55 cases (73%), the lowest energy pose is within 2.0 Å RMSD with respect to the X-ray PDB complex (see Table 1, Figure 1a and Discussion). The results are not dependent on the ideality of the bond lengths and angles in the molecule: the CORINA generated conformers show an almost identical behavior to the PDB based conformers. As for the remaining 27%, the program fails to obtain the correct binding mode as the lowest energy pose (shaded entries in Table 1). Among these, in 15 cases the binding mode is within 2.5 Å of the experimental solution. In 10 cases the algorithm finds a correct binding mode within the first 15 energy ranked solutions. Only in three cases does the algorithm fail to find correct solutions in the upper ranking list. When these failures were analyzed, we found that in most cases (as in 1aqw, 1mLd, 1tnk, 1ppc, 2tsc, 1mts, or 4dfr) the docked ligand largely overlaps

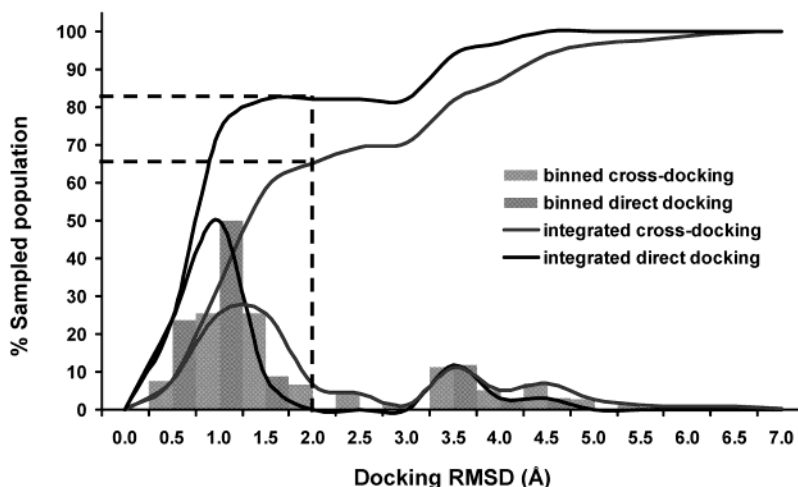


Figure 2. Histograms showing the docking RMSD (Å) distribution (RMSD of 2.0 Å or less is considered a successful solution) in a set of 34 neuraminidase–inhibitor complexes taken as representative congeneric series example.¹⁹ Direct docking (black) and cross-docking (gray) results are compared. Both binned (bars) and integrated (lines) distributions are shown.

with the experimental binding mode, but has one portion of the molecule in a different orientation. On the other hand, the programs failed completely in the recognition of the binding modes for 1bma and 1d0l.

Although difficult to quantify, different docking studies over different systems (data not shown) have allowed us to observe that as a general trend, successful docking runs tend to present more negative values of the VDW energy per heavy atom and a larger VDW energy gap (measured as the VDW energy difference between the model ranked first and the average of the next five poses). These energy values are shown for the docking models presented in Table 1. This tendency is in agreement with a funnellike view of the energy landscape in molecular recognition, with a predominant role of shape complementarity in selecting the binding mode.⁴⁹ As native interactions are on average stronger than non-native ones, increasingly larger decreases in energy are expected as the nativelike binding mode is approached.

Cross Docking Performance on a NA–Inhibitor Set. Many proteins undergo small side chain or even backbone movements upon ligand binding. In some extreme cases large loop movements or even domain shifts can be induced.^{50,51} This induced fit is potentially problematic for virtual screening computations, as in most cases there is only one crystal structure to be used during the screening process.⁵² Assessing the sensitivity of the predicted docking modes in relation to the extent of structural changes is therefore important. The impact that small conformational shifts may have on the docking performance of our algorithm was evaluated through cross-docking experiments of 28 derivatives of sialic acid and benzoic acid analogues as ligands into 34 X-ray protein structures of influenza NA taken from a series previously used in the application of the COMBINE analysis¹⁹ as well as from two additional PDB entries (see Methods). NA is known to exhibit small but significant induced fit effects upon ligand binding. Previous docking studies have indicated that some docking methods are sensitive to the induced fit effects present in the NA–inhibitor series of complexes.⁵³ On the other hand, a recent report by Birch et al. has showed a significantly robust and accurate

performance of GOLD on this application.⁵⁴ Thus, it was of interest to study the performance of our algorithm on this set.

The full set of 34 complexes was tested and the RMSD to the reference structures calculated. As shown in Figure 2, in 82% of the cases the algorithm correctly docks the ligand into the binding site of its experimental partner. This is better than the 73% success rate seen against the general test set, and slightly worse than the results (87%) obtained for the full set tested with GOLD.⁵⁶ As previously observed, when failures are present the predicted conformation largely overlaps with the experimental binding mode. The cross-docking experiments had a high success rate, even for ligands that are known to cause small but significant induced fit effects. Thus, considering all possible cross-docking cases, the algorithm found the experimental binding mode in 66% of the cases (Figure 2), although results varied significantly with the protein model. While some models produced consistently good binding modes (e.g., 82% of ligands correctly docked against bc6 conformation), others performed poorly on average (e.g., only 21% and 27% of ligands were correctly docked against 1ivd and 1ive, respectively). These differences might be related to either the quality of the X-ray structure or the degree of “promiscuity” of some cavities or both, as discussed by Birch and co-workers.⁵⁴ Taking into consideration the differences in the series, we can conclude that our algorithm appears to be fairly insensitive to small protein shifts whereas its sensitivity to induced shifts is similar to that described for GOLD (76% of success for the cross-docking into the protein structures of their full set), despite our use of a sharp 12–6 potential for the VDW interactions.

COMBINE Analysis of fXa Inhibitors. Docking of fXa Inhibitors. For the derivation of the QSAR model and all subsequent experiments, our first objective was to derive binding modes for all members in the set of 3-amidinobenzyl-1*H*-indole-2-carboxamide analogues published by Matter et al.¹ (Figure 3). Various protein structures were considered in order to study the dependence of the COMBINE analysis models on the structural variability of the receptor. PDB entries 1fjs,⁴⁵ 1f0r,⁴⁶ and 1xka⁴⁷ were selected. The series of 133

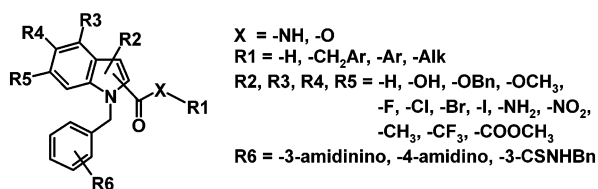


Figure 3. General structure of the series of 3-amidinobenzyl-1*H*-indole-2-carboxamides and analogues¹ used for our COMBINE analysis studies of the blood coagulation enzyme fXa inhibitory activity.

molecules was docked in each one of them following the procedures already described in the previous sections.

Before discussing our docking results, we briefly introduce the fXa binding site. The main determinant for the specificity of ligands toward proteins of the chymotrypsin-like family such as fXa is believed to be the deep S1 or specificity pocket.⁵⁵ The interior of the S1 pocket is fairly hydrophobic, except for the presence of the acidic carboxyl side chain of Asp189 (numbering scheme following chymotrypsin) at the bottom. This acidic group usually forms a salt bridge with positively charged ligand moieties, such as guanidinium groups, amines, or amidines. The catalytic triad, or S2 pocket, is formed by residues His57, Asp102, and Ser195. Additionally, the binding site possesses a S3 binding subsite, consisting of Gly216. Finally, there is a rather structured and mostly hydrophobic distal S4 region, lined by residues Tyr99, Phe174, Trp215, and Glu217, which is known as the aryl binding region. This pocket has been largely exploited in the design of selective fXa inhibitors.^{28,29} The arrangement of the binding site and a typical binding mode for members of the series studied here can be observed in Figure 4a. This binding mode is consistent with the available data. As shown by Matter et al.,¹ the amidinobenzyl at the indole N1 is located in the fXa S1 pocket, interacting with the basal Asp189. The indole scaffold itself is solvent-exposed, stacked against the flexible side chain of Gln192, and

involved in VDW contacts with the Cys191-Cys220 disulfide bond. The terminal group of the 3-amidinobenzyl-1*H*-indole-2-carboxamides and esters is situated in the S4 pocket, either parallel or perpendicular to the Trp215 indole ring, depending on its nature and substitution pattern.¹

Visual inspection of the docking results indicated that predictions were generally consistent with the canonical binding mode. However, and as expected based on the validation sets, some alternative docking modes were also found. Differences were also found depending on the PDB employed for the protein. 1Fjs docking modes were more homogeneous, commonly implicating either the standard mode or a reverse mode, inverted by 180° so that the benzamidine fragment occupied the S4 pocket while the distal ring was at the S1 subsite. This inverted mode was also the most frequent alternative pose at 1f0r enzyme cavity. As an example, the standard binding mode is shown for compound **34** (original series numbering¹) in Figure 4a, while the inverted pose for compound **30** is presented in Figure 4b, both docked to 1f0r. With 1f0r a similar fraction of canonical modes was observed compared to 1fjs, however, there was less homogeneity regarding alternative poses. Many solutions showed the benzamidine ring inside the S1 pocket, while the indole scaffold presented a different pose, perpendicularly situated with respect to the binding conformation shown in Figure 4a, and with the side chain connecting both lateral rings of the ligand structure pointing toward the S2 subsite, and leading also to a slightly different occupation of S4. Finally, 1xka showed the least “promiscuous” docking cavity. It is interesting to note that this is the structure solved at lower resolution. On the other hand, a linear correlation between the computed docking energy for the ligands and their fXa inhibitory activity was observed only for 1fjs-based models.

Chemometric Analysis. The same procedure was followed in parallel for each of the three sets of fXa-

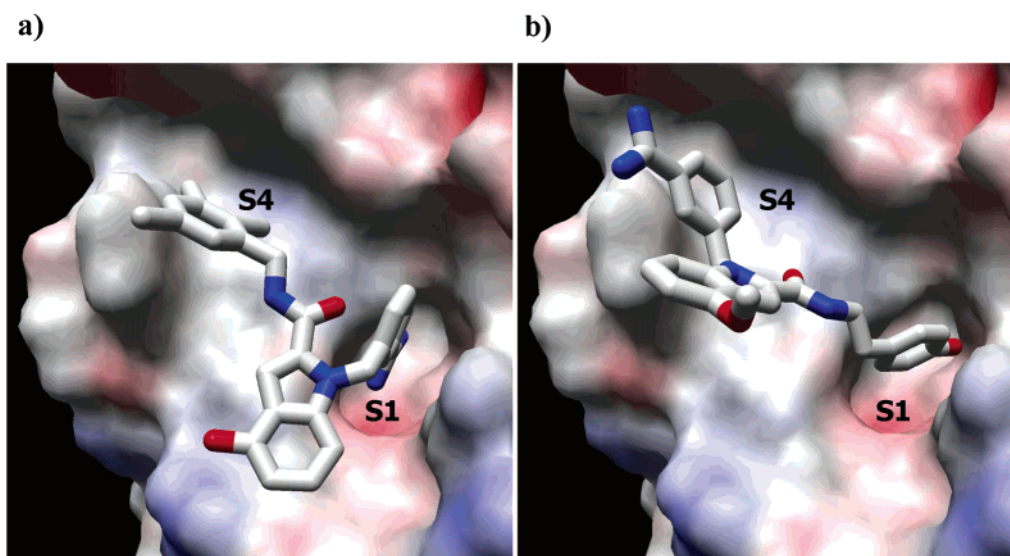


Figure 4. Details of binding models obtained for the studied indole derivatives as fXa inhibitors using our flexible docking algorithm. (a) Standard (correctly modeled) binding mode is shown for compound **34** (original series numbering) as an example, while for an (b) inverted type binding pose, compound **30** was chosen as an example. In both shown examples, 1f0r PDB entry was used for representing the fXa binding site. S1 and S4 denote subsites 1 and 4, respectively, in the binding site of fXa, as defined in ref 55. Note that occupancies of S1 and S4 pockets of the fXa binding site by the ligand benzamidine aromatic moiety and the distal aromatic subunit are inverted. Surface coloring scheme is according to the contributing atom.

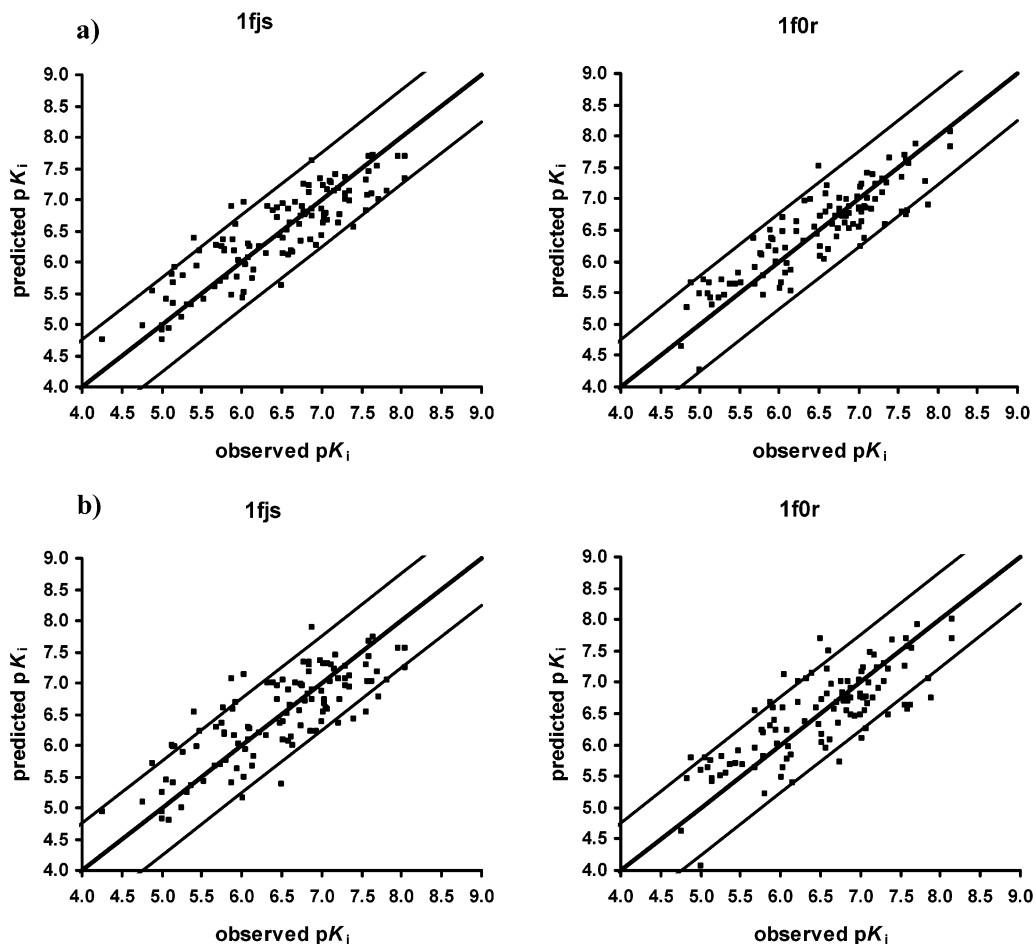


Figure 5. Predicted pK_i (a) fitted or (b) cross-validated, versus experimental pK_i for the fXa inhibitory activity for the 1fjs-based set (114 complexes) and the 1f0r-based set (107 complexes) included in the derivation of the corresponding COMBINE analysis model. The dark line corresponds to the regression line and the lighter lines mark deviations of $\pm 1.5 \cdot \text{SDEP}$ pK units.

inhibitor docking models (1fjs, 1f0r, and 1xka-based models). The predicted binding modes (see Methods for details) were used for the derivation of the QSAR model using COMBINE analysis. Initial PLS analyses, considering all 133 fXa inhibitors, gave low LOO Q^2 values in the range of 0.2–0.3. While this may point to some systematic errors in structural modeling or energy computation, it is most likely due to the presence of wrongly predicted docking modes for some inhibitors. Although PLS can cope with a certain amount of noise, the existence of these cases can compromise model derivation. In practice, a procedure must be implemented to cope with these cases by detecting likely wrong docking modes. Several approaches could have been used for this. We chose a self-consistent method where we assumed that significant deviation from the trend provided by the majority of the members in the sample most likely implies a wrong docking mode for the outlier. The best predictive model from this first run, as judged by Q^2 values in LOO cross-validation (1fjs-8 latent variables, $Q^2 = 0.317$, $R^2 = 0.564$; 1f0r-5 latent variables, $Q^2 = 0.214$, $R^2 = 0.404$; 1xka-3 latent variables, $Q^2 = 0.249$, $R^2 = 0.331$) was chosen, and compounds with unsigned errors of more than 1.2 pK_i units were removed from the training set, and a new PLS model was derived. The procedure was repeated until no outliers were found. In all cases three iterations were required, leaving 114 (1fjs), 107 (1f0r), and 113 (1xka)

compounds out of the initial set of 133. As expected, most of the outliers removed had docking modes inconsistent with the known binding modes. The statistical parameters corresponding to the 1fjs and 1f0r-based models at the optimal dimensionality of 8 are given in Table 2, while their fitted and predicted pK_i values are plotted against their experimental pK_i values in Figure 5. The poorer quality of the final 1xka-based regression model made us discard it for further applications ($Q^2 = 0.487$, $R^2 = 0.584$, $\text{SDEP} = 0.555$).

There is risk of over-fitting in the procedure applied to generate the final models, and appropriate tests must be used. To test the statistical significance of these models, scrambling tests were performed. Activity data were randomly scrambled 100 times producing 100 regression models. As can be seen in Figure 6, both models were robust according to the scramble runs. In a second test, external cross-validation was simulated by randomly taking 13 complexes out of the original dataset of 133 complexes to be used as a prediction or test set. The new training set of 120 inhibitors was used to build a model following the same protocol as applied to the whole dataset and the pK_i of the test set finally predicted with the purged training set. 20 of such test models were generated, using the same sets for 1fjs as well as for 1f0r-based COMBINE analysis validations. Models with similar internal predictive ability were obtained (1fjs – 3 to 8 latent variables, $Q^2 = 0.478$ to

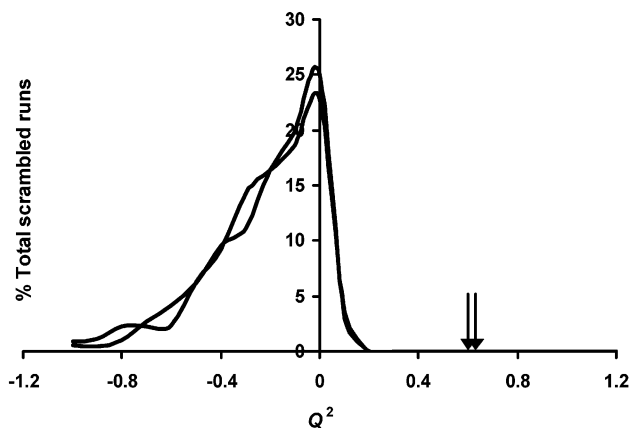


Figure 6. Histograms showing the cross-validated Q^2 value binned distribution for 100 regression models obtained after randomly scrambling the activity data. 1fjs-based models are shown in black while gray is used for the 1f0r-based models. Arrow lines mark the cross-validated Q^2 value for the real models.

0.642; 1f0r – 5 to 9 latent variables, $Q^2 = 0.502$ to 0.679). However, although validation by permutation confirms no chance correlation in these final models (Figure 6), the external predictive performances were proved to be not only worse than the internal, as expected, but really variable depending on the chosen external set due to the presence of some outliers (statistical data considering all compounds in the filtered external test sets: 1fjs: $Q^2 = 0.2060$, $R^2 = 0.3116$, SDEP = 0.7940; 1f0r: $Q^2 = 0.1029$, $R^2 = 0.2379$, SDEP = 0.8919). The cross-validated (both internally and externally) predicted pK_i values are plotted against experimental pK_i values for the 20 models in Figure 7. Overall, both 1fjs-based and 1f0r-based COMBINE analysis models produced reasonable predictions. This analysis indicates that it is possible to remove mis-docked solutions on the basis of the predictive ability in the context of the congeneric series, without producing a noticeable over-fit in the final models.

Virtual Screening Experiments. We generated a small in-house virtual library of 112 ligands (Tables A2 and A3, Supporting Information), containing both active and inactive compounds, as described in Methods. The AMBER energy-based and COMBINE analysis-based activity predictions are shown in Figure 8 in the form of ROC⁴⁸ plots. COMBINE analysis models improve the ability to identify structurally related molecules in external sets over the *naked* AMBER force field, achieving in our best case a recognition rate of ~80% of known binders at ~15% false positives rate. The performance with the 1f0r-based COMBINE analysis model was slightly better than the 1fjs-based one (Figure 8a) but, qualitatively, the results are similar. In the down side, it can also be observed that it is not possible to identify structurally unrelated inhibitors from those in the training series with COMBINE; pK_i predictions in this case are not significantly better than random (Figure 8b). Interestingly, the *naked* AMBER energy function has in this case some predictive ability for 1f0r-based models (Figure 8b).

The superiority of COMBINE analysis was also shown when the enrichment factors were analyzed (Figure 9). For members of the Matter et al. series, the COMBINE-based method achieved enrichment factors of 350–

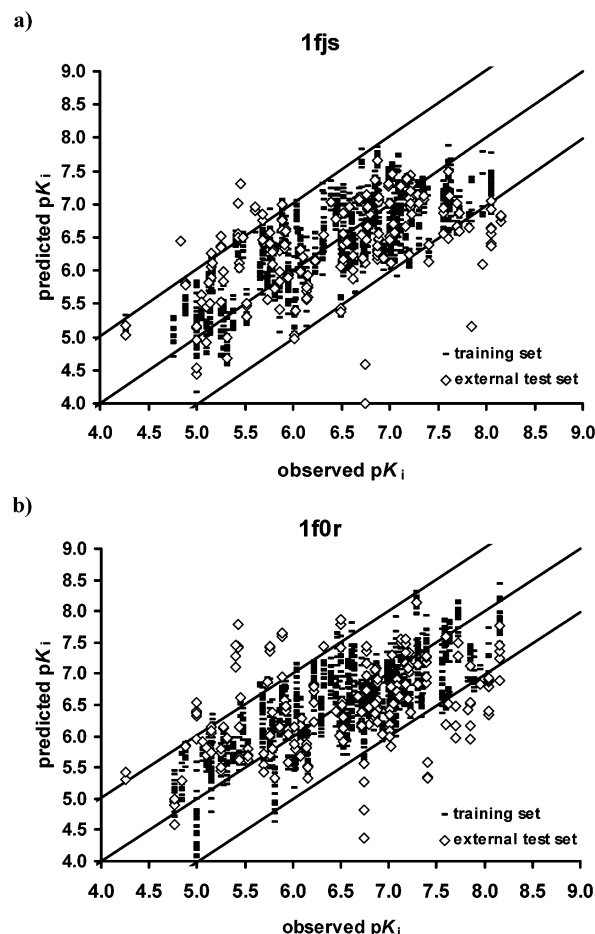
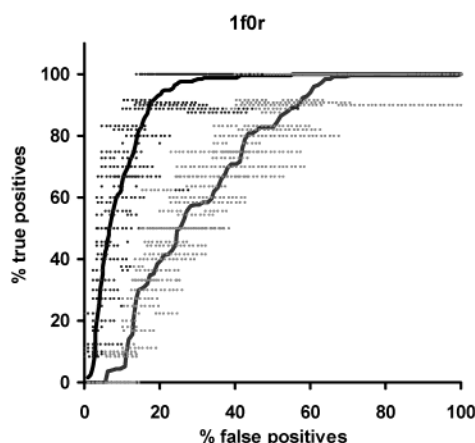
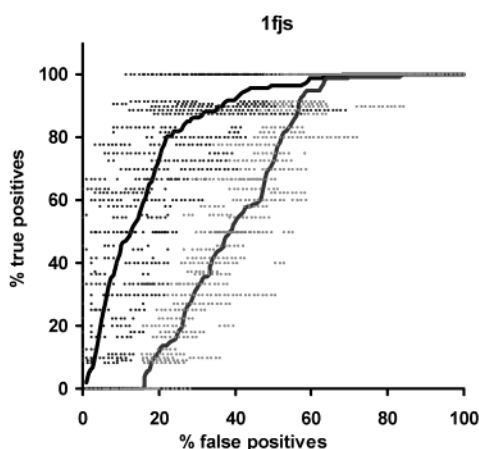


Figure 7. Cross-validated versus experimental pK_i for the inhibitors included in the training set (black dashes) and the corresponding inhibitors randomly extracted as a external set (white squares), using (a) 1fjs–inhibitor docking models or (b) 1f0r–inhibitor docking models for the COMBINE analysis derivation. The prediction data for each of the twenty randomly chosen external test sets of 13 inhibitors and the resulting internal training sets are shown together for each fXa PDB entry (see text for details). The dark line corresponds to a hypothetical perfect regression line ($x = y$) and the lighter lines mark deviations of $\pm 2 \cdot \text{SDEP } pK$ units (SDEP values are taken from the full models).

450%, depending on the receptor structure used, whereas the AMBER-only energy function produced poorer results.

Insights into FXa Inhibition. We used a threshold of 0.05/–0.05 on the PLS coefficients*STD to extract “important” VDW variables (Figure 10a), i.e., variables that are relevant to explain the activity differences across the series. VDW variables above the threshold in both COMBINE analysis models come from residues Ala190, Arg222, Gln192, Glu217, Gly216, Phe174, and Tyr99. Gly219 and Thr98 are important in 1fjs-based COMBINE analysis models, while for 1f0r-based analysis their contributions are not significant; His57, and to some extent Gln61, are more relevant in the 1f0r-based model. On the other hand, electrostatic variables above our selected threshold (0.1/–0.1, see Figure 10b) come mostly from charged residues: Arg143, Arg222, Asp102, Asp189, Asp194, Glu217, Glu97, Ile16, and Lys96. Specific to the 1fjs model are: Asp100, Lys148, Lys156, Lys224, and Trp215. On the other side, Glu147 is relevant only in the 1f0r-based model.

a) series members



b) non-series members

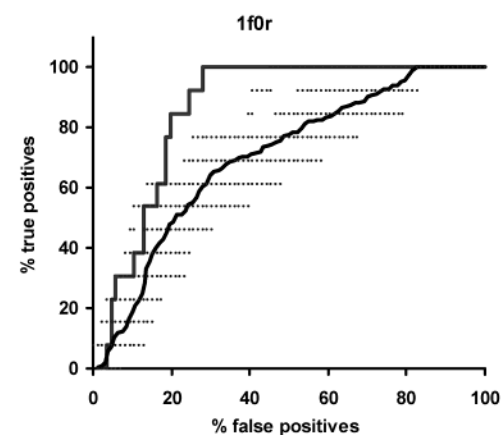
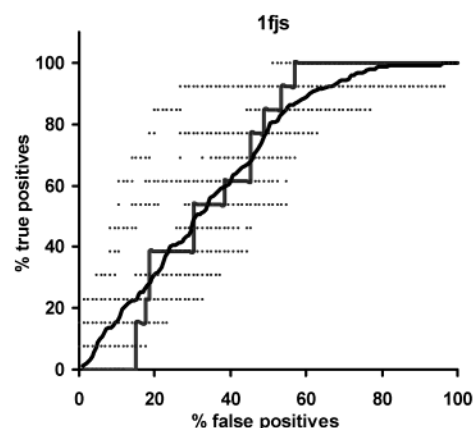


Figure 8. Receiver Operating Characteristic (ROC) plots for the fXa inhibitory activity detection in virtual screening experiments of our “toy library”: (a) series members fXa ligands and (b) fXa inhibitors nonstructurally related to the series. Both, 1fjs-based models and 1f0r-based models are shown. Molecules were ranked using two different scoring schemes: docking energy score (gray line) and COMBINE analysis externally predicted (pK_i) (black line). The percentage of successfully found binders (true positives) is scanned through the ranked database and plotted (points) as a function of the percentage of false positives accumulated for each one of the randomly chosen test sets. The average plot (lines) is also shown (see text for details).

As can be observed in Figure 10, the most influential variables are correlated in both models. However, there are also a few terms with considerably larger significance in one model than in the other. For example, the VDW contribution of Gln192 and Gly219 is larger with 1fjs than with 1f0r, while the opposite occurs with Gly216 (Figure 10a). More notable is the different behavior in the electrostatic interactions profiles, particularly for residues of Arg222, Glu217, Asp102, Arg143, and Glu147 (Figure 10b). In Figure 10c we show the most prominent differences within the structural context. Note the different conformation of the S4 aromatic box in 1fjs and 1f0r. Both Phe174 and Tyr99 side chains are displaced in the same direction giving a shifted configuration for their location. This relative *swing* movement might affect the affinity contribution profile of residues close to the benzenic side chains that have the same or similar side chain conformation in both X-ray structures, namely Glu217 and more strikingly His57, Thr98, and Asp102. The side chain of Gln192, located at the entrance of the S1 pocket, is also notably different in the two PDB entries employed, as well as Gln61, and to a lesser extent Arg143 and Arg222 side chains. Other residues having notably different contributions are second-shell charged residues such as

Glu97, Lys96, Lys148, Lys156, Lys224, and Glu147. Therefore, while qualitative analysis of regression coefficients is robust to the different conformational sub-states of the receptor, quantitative analysis is not warranted.

Finally, a view of the electrostatic and VDW energy contributions selected by COMBINE analysis at the fXa binding site is shown in Figure 11. It is reassuring that all pockets known to be required for inhibition with this series are selected, namely the S1 pocket in the neighborhood of Asp189, including Arg143, Arg222, Gly219, and Gln192 amino acids; the S4 pocket containing the aromatic box and Glu217; the S2 region; and to a minor extent the interaction with the backbone through residue Gly216, known as the S3 area.

Discussion

A two-step, fully automated procedure consisting of ligand–receptor docking and affinity prediction using COMBINE analysis is presented as a useful method for lead optimization, including virtual screening-based optimization. This is exemplified with a set of fXa inhibitors,¹ selected as a realistic model for lead optimization. Complexes were generated by automatically docking the ligands into fXa binding sites, solved with

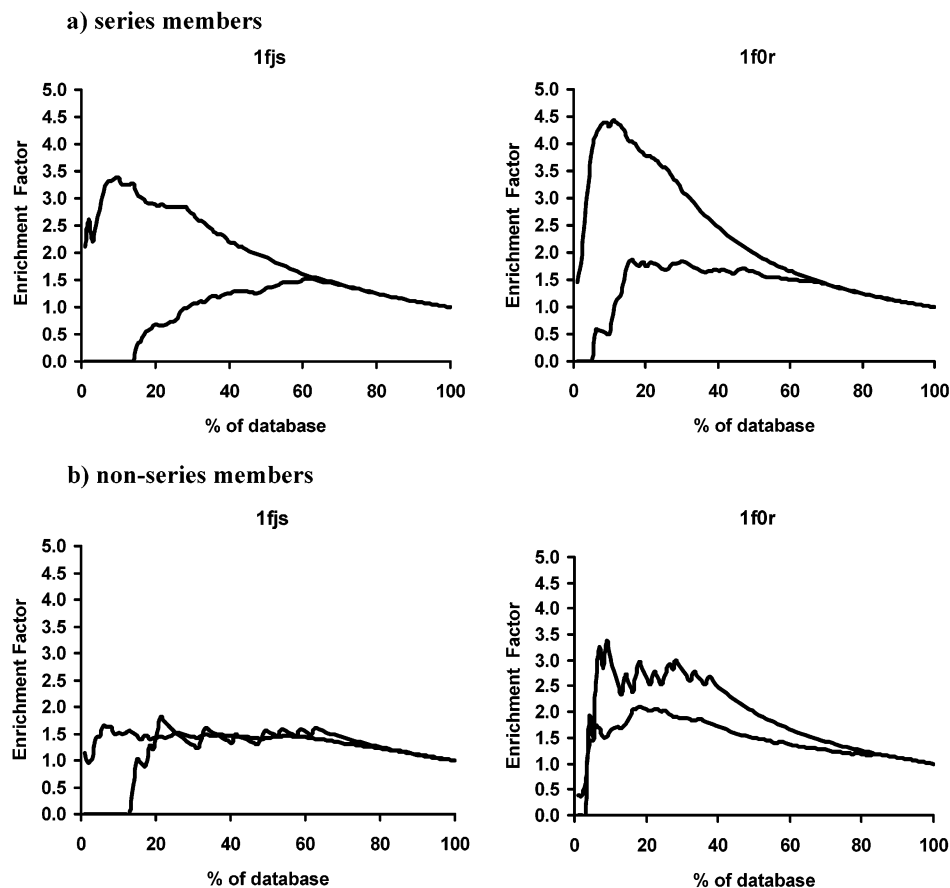


Figure 9. Enrichment factor for the fXa inhibitory activity detection in virtual screening experiments of our “toy library” scanned through the ranked database: (a) series members fXa ligands and (b) fXa inhibitors nonstructurally related to the series. Both, 1fjs-based models and 1f0r-based models are shown. Molecules were ranked using two different scoring schemes: docking energy score (gray line) and COMBINE analysis externally predicted (cross validated) pK_i (black line). The enrichment factor (concentration of found binders in subset/concentration of binders in database) is computed through the ranked database for the randomly chosen test set (see text for details).

proteins bound to structurally unrelated ligands. The series is large (133 members), as it would be expected on an ongoing drug discovery program.

The first step in the procedure makes use of an automatic docking algorithm. We have applied a deterministic approach, splitting up the conformational space into quantized units by only considering torsional degrees of freedom and fixing each torsional angle into coarse rotameric states (see Methods). By doing this, we are certain we can select the lowest energy pose with our scoring function at a given level of discretization, but this comes with a price. There is a risk of missing conformations that are outside the defined torsional space.³⁶ However, and despite the coarse set of angles employed, the strategy has proved surprisingly robust and successful, as exemplified by the 73% success rate in our set of 55 different complexes. This is similar to or better than the success rates reported for the most successful docking algorithms over large datasets. For example, studies with GOLD have reported a 71% success rate out of a list of 100 examples,⁵⁶ while similar studies with FlexX have reported only 46.5% in a 200 compounds database,⁵⁷ although Gohlke et al. presented a substantial improvement within FlexX by reranking the poses with DrugScore. In this case, 75% of the cases, using two datasets of 91 and 68 complexes, were predicted correctly.⁵⁸ Finally, Surflex,⁵⁹ a flexible docking algorithm that combines the scoring function from

Hammerhead⁶⁰ with a search engine that relies on a surface-based molecular similarity method, obtained ~70% success rate on a list of 81 complexes. As an additional test to validate the docking results, we selected from published data for these programs a set of 53 complexes reproducing the rotatable bond distribution of Table 1 (for GOLD data were taken from http://www.ccdc.cam.ac.uk/prods/gold/rms_tab.html; for FlexX data were downloaded from <http://www.biosolveit.de/FlexX>; and for Surflex data were selected from the original reference). Using our criteria of success we obtained the following success rates for the different programs: 79% (Surflex); 77% (Gold); 53% (FlexX). This should be compared with the 73% success rate of our program.

Although we were initially surprised with the performance of the algorithm using such a naïve approach, other groups have documented similar observations. For example, Richards and co-workers have also recently shown that it is possible to discretize the search space in very coarse “chunks” and yet achieve successful docking predictions.⁶¹ Similarly to us, they employ a coarse set of rotameric states, in their case with a step size of 60°. A flexible ligand docking protocol that uses a grid-based method to sample the conformation of an unbound ligand and to select the low-energy conformers, followed by rigid docking and structure refinement has been also successfully applied by Wang et al.⁶²

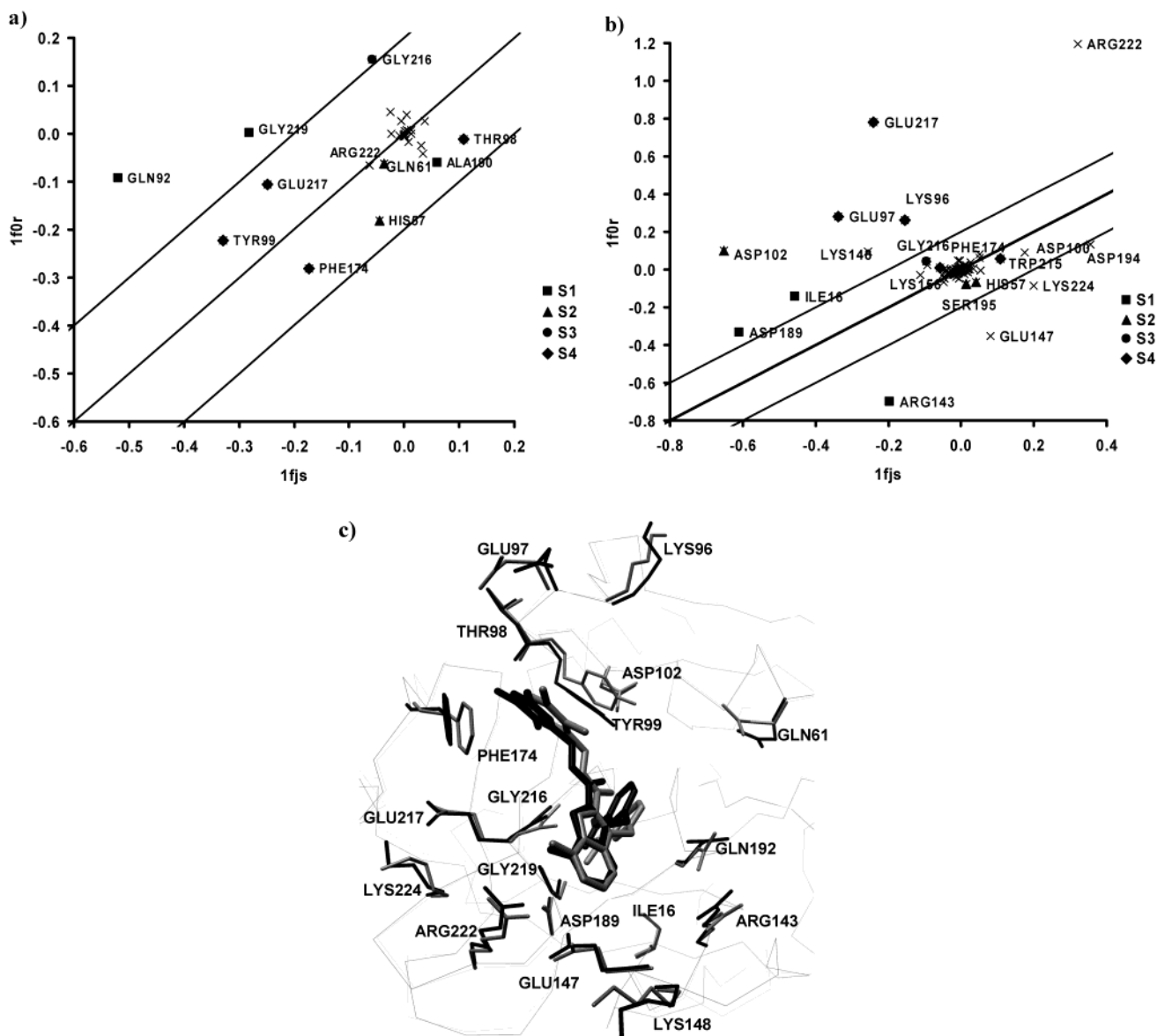


Figure 10. (a) VDW and (b) electrostatic PLS coefficients*STD in the 1fjs- versus 1f0r-based COMBINE analysis models. Residues with high coefficients are labeled. (c) Residues behaving in a different manner in both models shown at the fXa binding site. Compound **34** is shown as an example. Gray color is used for 1fjs PDB, while black is employed for highlighting 1f0r side chains.

Obviously, there were some failures clearly due to this representation. For example, 3ert (human estrogen receptor α ligand-binding domain in complex with 4-hydroxytamoxifen) can be successfully docked only after introducing, together with the default values of 90° and 0° , an additional rotameric state at 45° for dihedral angles $\text{Csp}^2(\text{benzene})-\text{Csp}^2(\text{benzene})-\text{C}=\text{C}$. Similarly, in 1tni (trypsin complexed with the inhibitor 4-phenylbutylamine) the presence of an eclipsed conformation on the central $\text{Csp}^3-\text{Csp}^3$ bond in the crystal structure cannot be reproduced by our default set of torsional angles. The simplification affects negatively large, flexible molecules, where dihedral deviation from ideal values are transmitted throughout the structure and, due to leverage, amplified at distant positions. A second, related risk with the enumeration approach is combinatorial explosion. Highly flexible compounds, with a large number of conformers, cannot be evaluated exhaustively. Both factors add up, so that molecules having eight or more rotatable bonds are difficult to dock by our method (Table 1). Nevertheless, for most

druglike rule-of-five-compliant molecules, this is not a problem, and computing times are kept manageable. For typical ligands, and considering that the algorithm needs ~ 10 s per sampled conformation (Figure 1b), flexible docking requires of the order of minutes on a desktop workstation. The approach seems accurate and robust enough for virtual screening applications. Tolerance to small structural shifts in the receptor is observed, as exemplified with the NA dataset, where our results are similar to those obtained with GOLD,⁵⁵ and an improvement over those previously reported with PRO_LEADS.⁵³ Thus, the algorithm seems able to handle minor conformational changes, while still taking advantage of the rigid protein approximation.

When considering the docked models of the 133 series of fXa inhibitors, it was reassuring to verify that they were, for the most part, consistent with the expected orientation for this set of compounds.¹ Alternative binding modes were also found, usually consisting of a 180° rotation that involves an interchange of the moieties interacting at S1 and S4 subsites (Figure 4).

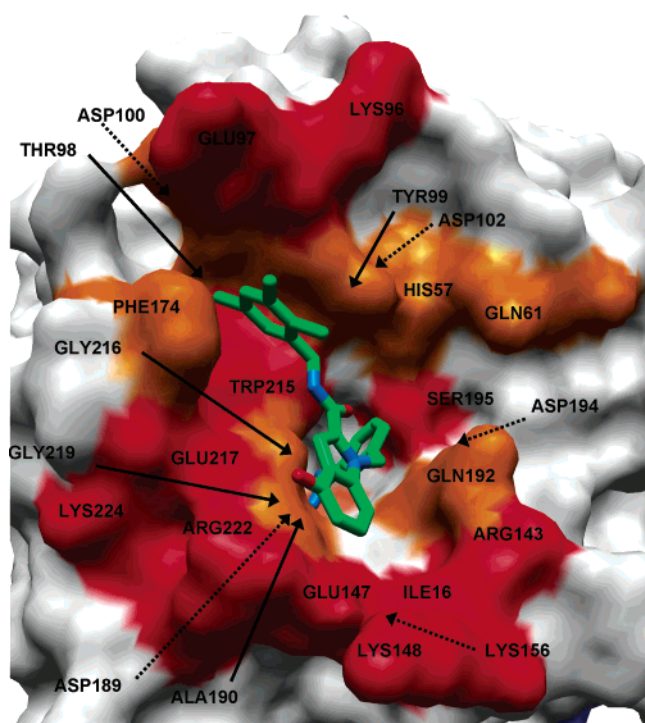


Figure 11. COMBINE analysis coefficients mapping into the fXa binding site. Relevant residues for VDW interaction are colored in orange, while red is used for electrostatically important residues. Compound **34** is shown as an example.

The fraction of the series inhibitors docked in such a way is of approximately 30% for 1fjs and 1f0r based docking models, and slightly lower (%20) for the 1xka ones. Interestingly, Mikol and co-workers have recently reported crystal structures for a series of sulfonylpiperazinones bound in the same reverse orientation, with neutral groups occupying the S1 pocket while basic moieties, including benzamidine rings, bind to S4, indicating that formation of a salt bridge in S1 is not an absolute prerequisite for high affinity.⁶³ While it is likely that the scaffold in the ligand, among other factors, influences equilibrium between both binding modes, our results suggest that there is a possibility that some of the inhibitors in our series can also bind using this reverse mode.

Turning to the regression models, it is of interest to note that only two (1fjs and 1f0r-based) of the three initially developed COMBINE analyses proved predictive (Table 2, Figures 5 and 7). We ascribe this result to poorer docking models with 1xka than with the other two proteins, likely caused by the conformational sub-state of 1xka or its lower experimental resolution. Analyzing the two predictive models, we observe that, as expected, prediction of inhibitory activity in the external test sets is better for compounds that are similar to those in the training set. External predictions are shown in Figure 7. Based on energy-landscape criteria of what is or is not most likely to be a correct binding mode, the study of the docking models obtained for the fXa inhibitors in the three PDB based-employed conformations for the enzyme, made it possible to establish an energy cutoff value for the energy gap and the average VDW energy per heavy atom as filter for the docking models obtained in this system. Thus, only compounds docked with a positive value for the VDW energy gap and a VDW docking energy per number of

ligand heavy atoms lower than -1.2 kcal/mol were selected as reliably docked conformations.

Comparing the results with both scoring systems, it can be concluded that COMBINE analysis provides good predictive abilities and a moderate degree of robustness against fluctuations in the protein structure when addressing congeneric series optimization, while the *naked* AMBER energy function is less predictive and more dependent on the specific details of the protein conformation. On the negative side, when the objective was the identification of structurally unrelated inhibitors (i.e., new leads), only the *naked* AMBER energy showed some predictive ability, and only with one of the receptor conformations (1f0r, see Figures 8b and 9b). We caution, however, that a limitation in this part of the study is the small size of the library being used, which translates into considerably fluctuations in the computed plots (Figures 8 and 9). Nevertheless, the salient features of our study seem to be robust enough, and independent of these fluctuations.

Mechanistic interpretations of COMBINE analysis models have been previously used to help understanding SARs.^{12,13,21} Here we have taken the opportunity to check the consistency of such interpretations for the fXa inhibitor series, by comparing the results in the two different receptor conformations. The examination of the regression coefficients plot (Figure 10), along with the structures of the ligand–receptor complexes (Figures 4 and 11), can pinpoint key interactions responsible, in a statistical sense, of the differences in affinity. As can be observed in Figure 10, 1fjs and 1f0r roughly share the same set of relevant variables to explain affinity. However, there are a few terms playing a substantially more prominent role in one model than in the other (see Results for details). Thus, although affinity factors can be rationalized and dissected to a certain extent, care must be taken when attempting quantitative analysis to avoid overinterpretation. The derived regression models are conformation dependent, and in the absence of conformational sampling in the receptor are more adequate for qualitative reasoning. This is particularly important if insights extracted from the analysis are going to be used in the next round of ligand design. Our results suggest that in those cases it may be wise to confirm the relevance of the interactions by repeating the analysis with alternative conformations of the receptor, either experimentally available or extracted from a molecular dynamics trajectory.

Conclusions

A new protocol is presented for virtual screening-based lead optimization in receptor-based drug design, and applied to a series of recently reported fXa inhibitors. A docking algorithm is used to generate ligand–receptor complexes that are analyzed using COMBINE analysis to obtain SARs in the context of the interaction energetics. While more research is required, the approach holds considerable promise in the problem of optimizing leads using virtual libraries.

Our findings suggest that ligand screening using force field energies and COMBINE analysis could be used complementarily. The use of *naked* docking energies seems to be more adequate for screening general databases or creating targeted libraries during a lead

discovery program, where diverse scaffolds need to be identified. In contrast, COMBINE analysis predictions are better suited for screening focused libraries during a lead optimization program, where a scaffold has already been defined. Mixing both scoring schemes can also be advantageous from a computational standpoint. A useful strategy worth pursuing would be to dock and score libraries using the standard force field and then to rerank the upper ~15% or so of the list with the COMBINE analysis methodology.

Reliable docking has been shown to be, as expected, a key ingredient. Here, we have taken an approach different from most available docking algorithms in that we have tried to exhaustively enumerate receptor–ligand orientations using a rather drastic discretization of conformational space. Although we were initially surprised with the performance of the algorithm using such a naïve approach, other groups have recently documented similar observations.^{61,62} Finally, while dependencies of the COMBINE analysis models on receptor conformation have been detected, the docking algorithm itself is reasonably insensitive to small structural shifts in the receptor, as exemplified with the cross-docking experiments using the NA dataset. If the purpose of the COMBINE analysis is to obtain mechanistic insights about the inhibition process, introduction of protein flexibility⁵¹ is most likely required to establish consistency.

Acknowledgment. These datasets will be made electronically available in our web page (<http://bioinf5.cbm.uam.es>). Meanwhile, they are available from the authors (aro@cbm.uam.es). M.M. was partially supported by a postdoctoral fellowship from *Fundación Ramón Areces*. We thank Dr. Hans Matter from Aventis Pharma for making available to us some of his data. We also thank Dr. Federico Gago for carefully reading the manuscript. This work has been supported by grants from MCYT and FIS and by an institutional grant from Fundación Ramón Areces to Centro de Biología Molecular “Severo Ochoa”.

Supporting Information Available: Tables 1A–3A. This material is available free of charge via the Internet at <http://pubs.acs.org>.

References

- Matter, H.; Defossa, E.; Heinelt, U.; Blohm, P. M.; Schneider, D. et al. Design and quantitative structure–activity relationship of 3- amidinobenzyl-1H-indole-2-carboxamides as potent, non-chiral, and selective inhibitors of blood coagulation factor Xa. *J. Med. Chem.* **2002**, *45*, 2749–2769.
- Rowland, R. S. Using X-ray crystallography in drug discovery. *Curr. Opin. Drug Discovery Dev.* **2002**, *5*, 613–619.
- Neamati, N.; Barchi, J. J., Jr. New paradigms in drug design and discovery. *Curr. Top Med. Chem.* **2002**, *2*, 211–227.
- Gohlke, H.; Klebe, G. Approaches to the description and prediction of the binding affinity of small-molecule ligands to macromolecular receptors. *Angew Chem., Int. Ed.* **2002**, *41*, 2644–2676.
- Buchanan, S. G. Structural genomics: bridging functional genomics and structure-based drug design. *Curr. Opin. Drug Discovery Dev.* **2002**, *5*, 367–381.
- Broder, S.; Venter, J. C. Sequencing the entire genomes of free-living organisms: the foundation of pharmacology in the new millennium. *Annu. Rev. Pharmacol. Toxicol.* **2000**, *40*, 97–132.
- Agrafiotis, D. K.; Lobanov, V. S.; Salemme, F. R. Combinatorial informatics in the post-genomics ERA. *Nat. Rev. Drug Discovery* **2002**, *1*, 337–346.
- Halperin, I.; Ma, B.; Wolfson, H.; Nussinov, R. Principles of docking: An overview of search algorithms and a guide to scoring functions. *Proteins* **2002**, *47*, 409–443.
- Brooijmans, N.; Kuntz, I. D. Molecular Recognition and Docking Algorithms. *Annu. Rev. Biophys. Biomol. Struct.* **2003**, *28*, 28.
- Schneider, G.; Bohm, H. J. Virtual screening and fast automated docking methods. *Drug Discovery Today* **2002**, *7*, 64–70.
- Taylor, R. D.; Jewsbury, P. J.; Essex, J. W. A review of protein-small molecule docking methods. *J. Comput. Aided. Mol. Des.* **2002**, *16*, 151–166.
- Ortiz, A. R.; Pisabarro, M. T.; Gago, F.; Wade, R. C. Prediction of drug binding affinities by comparative binding energy analysis. *J. Med. Chem.* **1995**, *38*, 2681–2691.
- Wade, R. C. Derivation of QSARs using 3D structural models of protein–ligand complexes by COMBINE analysis. *Rational Approaches to Drug Design: 13th European Symposium on Quantitative Structure–Activity Relationships*; Prous Science S. A.: Barcelona, 2001; pp 23–28.
- Cornell, W. D.; Cieplak, P.; Bayly, C. I.; Gould, I. R.; Merz, K. M. et al. A Second generation force field for the simulation of proteins, nucleic acids, and organic molecules. *J. Am. Chem. Soc.* **1995**, *117*, 5179–5197.
- Cuevas, C.; Pastor, M.; Perez, C.; Gago, F. Comparative binding energy (COMBINE) analysis of human neutrophil elastase inhibition by pyridone-containing trifluoromethyl ketones. *Comb. Chem. High Throughput Screen* **2001**, *4*, 627–642.
- Ortiz, A. R.; Pastor, M.; Palomer, A.; Cruciani, G.; Gago, F.; et al. Reliability of comparative molecular field analysis models: effects of data scaling and variable selection using a set of human synovial fluid phospholipase A2 inhibitors. *J. Med. Chem.* **1997**, *40*, 1136–1148.
- Pastor, M.; Perez, C.; Gago, F. Simulation of alternative binding modes in a structure-based QSAR study of HIV-1 protease inhibitors. *J. Mol. Graph. Model.* **1997**, *15*, 364–371, 389.
- Perez, C.; Pastor, M.; Ortiz, A. R.; Gago, F. Comparative binding energy analysis of HIV-1 protease inhibitors: incorporation of solvent effects and validation as a powerful tool in receptor-based drug design. *J. Med. Chem.* **1998**, *41*, 836–852.
- Wang, T.; Wade, R. C. Comparative binding energy (COMBINE) analysis of influenza neuraminidase-inhibitor complexes. *J. Med. Chem.* **2001**, *44*, 961–971.
- Lozano, J. J.; Pastor, M.; Cruciani, G.; Gaedt, K.; Centeno, N. B. et al. 3D-QSAR methods on the basis of ligand–receptor complexes. Application of COMBINE and GRID/GOLPE methodologies to a series of CYP1A2 ligands. *J. Comput. Aided Mol. Des.* **2000**, *14*, 341–353.
- Kmunicek, J.; Luengo, S.; Gago, F.; Ortiz, A. R.; Wade, R. C.; et al. Comparative binding energy analysis of the substrate specificity of haloalkane dehalogenase from *Xanthobacter autotrophicus* GJ10. *Biochemistry* **2001**, *40*, 8905–8917.
- Tomic, S.; Kojic-Prodic, B. A quantitative model for predicting enzyme enantioselectivity: application to Burkholderia cepacia lipase and 3-(aryloxy)-1,2-propanediol derivatives. *J. Mol. Graph. Model.* **2002**, *21*, 241–252.
- Tomic, S.; Nilsson, L.; Wade, R. C. Nuclear receptor-DNA binding specificity: A COMBINE and Free-Wilson QSAR analysis. *J. Med. Chem.* **2000**, *43*, 1780–1792.
- Wang, T.; Wade, R. C. Comparative binding energy (COMBINE) analysis of OppA-peptide complexes to relate structure to binding thermodynamics. *J. Med. Chem.* **2002**, *45*, 4828–4837.
- Leadley, R. J., Jr. Coagulation factor Xa inhibition: biological background and rationale. *Curr. Top Med. Chem.* **2001**, *1*, 151–159.
- Porcari, A. R.; Chi, L.; Leadley, R. Recent advances in clinical trials of the direct and indirect selective Factor Xa inhibitors. *Expert Opin. Investig. Drugs* **2000**, *9*, 1595–1600.
- Davie, E. W.; Fujikawa, K.; Kisiel, W. The coagulation cascade: initiation, maintenance, and regulation. *Biochemistry* **1991**, *30*, 10363–10370.
- Pauls, H. W.; Ewing, W. R. The design of competitive, small-molecule inhibitors of coagulation factor Xa. *Curr. Top Med. Chem.* **2001**, *1*, 83–100.
- Quan, M. L.; Wexler, R. R. The design and synthesis of noncovalent factor Xa inhibitors. *Curr. Top Med. Chem.* **2001**, *1*, 137–149.
- Wang, J.; Cieplak, P.; Kollman, P. A. How well does a restrained electrostatic potential (RESP) model perform in calculating conformational energies of organic and biological molecules? *J. Comput. Chem.* **2000**, *21*, 1049–1074.
- Perez, C.; Ortiz, A. R. Evaluation of docking functions for protein–ligand docking. *J. Med. Chem.* **2001**, *44*, 3768–3785.
- Besler, B. H.; Merz, K. M.; Kollmann, P. A. Atomic charges derived from semiempirical methods. *J. Comp. Chem.* **1990**, *11*, 431–439.
- Dewar, M. J. S. Z.; Eve G.; Healy, Eamonn F.; Stewart, James J. P. Development and use of quantum mechanical molecular models. 76. AM1: a new general purpose quantum mechanical molecular model. *J. Am. Chem. Soc.* **1985**, *107*, 3902–3909.
- Stewart, J. J. MOPAC: a semiempirical molecular orbital program. *J. Comput. Aided Mol. Des.* **1990**, *4*, 1–105.
- MOPAC 93; J. J. P. Stewart and Fujitsu Limited: Tokyo, Japan.

- (36) Bostrom, J. Reproducing the conformations of protein-bound ligands: a critical evaluation of several popular conformational searching tools. *J. Comput. Aided Mol. Des.* **2001**, *15*, 1137–1152.
- (37) Nelder, J. A.; Mead, R. A simplex method for function minimization. *Computer J.* **1965**, *7*, 308–313.
- (38) Bernstein, F. C.; Koetzle, T. F.; Williams, G. J.; Meyer, E. E.; Brice, M. D. et al. The Protein Data Bank: a computer-based archival file for macromolecular structures. *J. Mol. Biol.* **1977**, *112*, 535–542.
- (39) Case, D. A.; D. A. P.; Caldwell, J. W.; Cheatham, T. E., III; Wang, J.; Ross, W. S.; Simmerling, C.; Darden, T.; Merz, K. M.; Stanton, R. V.; Cheng, A.; Vincent, J. J.; Crowley, M.; Tsui, V.; Gohlke, H.; Radmer, R.; Duan, Y.; Pitera, J.; Massova, I.; Seibel, G. L.; Singh, U. C.; Weiner, P.; Kollman, P. A. *AMBER 7*; University of California: San Francisco.
- (40) *InsightII version 2000*; Molecular Simulations, Inc.: San Diego, CA.
- (41) Sadowski, J.; Gasteiger, J.; Klebe, G. Comparison of Automatic Three-dimensional Model Builders Using 639 X-Ray Structures. *J. Chem. Inf. Comput. Sci.* **1994**, *34*, 1000–1008.
- (42) Sadowski, J.; Gasteiger, J. From Atoms and Bonds to Three-dimensional Atomic Coordinates: Automatic Model Builders. *Chem. Rev.* **1993**, *93*, 2567–2581.
- (43) Ortiz, A. R.; Strauss, C. E.; Olmea, O. MAMMOTH (matching molecular models obtained from theory): an automated method for model comparison. *Protein Sci.* **2002**, *11*, 2606–2621.
- (44) Wold, S.; Ruhe, A.; Wold, H.; Dunn, W. J., III. The collinearity problem in linear regression: the partial least squares (PLS) approach to generalized inverses. *SIAM J. Sci. Stat. Comp.* **1984**, *5*, 735–743.
- (45) Adler, M.; Davey, D. D.; Phillips, G. B.; Kim, S. H.; Jancarik, J.; et al. Preparation, characterization, and the crystal structure of the inhibitor ZK-807834 (CI-1031) complexed with factor Xa. *Biochemistry* **2000**, *39*, 12534–12542.
- (46) Maignan, S.; Guilloteau, J. P.; Pouzieux, S.; Choi-Sledeski, Y. M.; Becker, M. R.; et al. Crystal structures of human factor Xa complexed with potent inhibitors. *J. Med. Chem.* **2000**, *43*, 3226–3232.
- (47) Kamata, K.; Kawamoto, H.; Honma, T.; Iwama, T.; Kim, S. H. Structural basis for chemical inhibition of human blood coagulation factor Xa. *Proc. Natl. Acad. Sci. U.S.A.* **1998**, *95*, 6630–6635.
- (48) Baldi, P.; Brunak, S.; Chauvin, Y.; Andersen, C. A.; Nielsen, H. Assessing the accuracy of prediction algorithms for classification: an overview. *Bioinformatics* **2000**, *16*, 412–424.
- (49) Verkhivker, G. M.; Rejto, P. A.; Gehlhaar, D. K.; Freer, S. T. Exploring the energy landscapes of molecular recognition by a genetic algorithm: analysis of the requirements for robust docking of HIV-1 protease and FKBP-12 complexes. *Proteins* **1996**, *25*, 342–353.
- (50) Fradera, X.; De La Cruz, X.; Silva, C. H.; Gelpi, J. L.; Luque, F. J.; et al. Ligand-induced changes in the binding sites of proteins. *Bioinformatics* **2002**, *18*, 939–948.
- (51) Wong, C. F.; McCammon, J. A. Protein flexibility and computer-aided drug design. *Annu. Rev. Pharmacol. Toxicol.* **2003**, *43*, 31–45.
- (52) Carlson, H. A.; McCammon, J. A. Accommodating protein flexibility in computational drug design. *Mol. Pharmacol.* **2000**, *57*, 213–218.
- (53) Murray, C. W.; Baxter, C. A.; Frenkel, A. D. The sensitivity of the results of molecular docking to induced fit effects: application to thrombin, thermolysin and neuraminidase. *J. Comput. Aided Mol. Des.* **1999**, *13*, 547–562.
- (54) Birch, L.; Murray, C. W.; Hartshorn, M. J.; Tickle, I. J.; Verdonk, M. L. Sensitivity of molecular docking to induced fit effects in influenza virus neuraminidase. *J. Comput. Aided Mol. Des.* **2002**, *16*, 855–869.
- (55) Maignan, S.; Mikol, V. The use of 3D structural data in the design of specific factor Xa inhibitors. *Curr. Top Med. Chem.* **2001**, *1*, 161–174.
- (56) Jones, G.; Willett, P.; Glen, R. C.; Leach, A. R.; Taylor, R. Development and validation of a genetic algorithm for flexible docking. *J. Mol. Biol.* **1997**, *267*, 727–748.
- (57) Kramer, B.; Rarey, M.; Lengauer, T. Evaluation of the FLEXX incremental construction algorithm for protein-ligand docking. *Proteins* **1999**, *37*, 228–241.
- (58) Gohlke, H.; Hendlich, M.; Klebe, G. Knowledge-based scoring function to predict protein-ligand interactions. *J. Mol. Biol.* **2000**, *295*, 337–356.
- (59) Jain, A. N. Surflex: fully automatic flexible molecular docking using a molecular similarity-based search engine. *J. Med. Chem.* **2003**, *46*, 499–511.
- (60) Welch, W.; Ruppert, J.; Jain, A. N. Hammerhead: fast, fully automated docking of flexible ligands to protein binding sites. *Chem. Biol.* **1996**, *3*, 449–462.
- (61) Glick, M.; Grant, G. H.; Richards, W. G. Docking of flexible molecules using multiscale ligand representations. *J. Med. Chem.* **2002**, *45*, 4639–4646.
- (62) Wang, J.; Kollman, P. A.; Kuntz, I. D. Flexible ligand docking: a multistep strategy approach. *Proteins* **1999**, *36*, 1–19.
- (63) Maignan, S.; Guilloteau, J. P.; Choi-Sledeski, Y. M.; Becker, M. R.; Ewing, W. R. et al. Molecular structures of human factor Xa complexed with ketopiperazine inhibitors: preference for a neutral group in the S1 pocket. *J. Med. Chem.* **2003**, *46*, 685–690.
- (64) Brandstetter, H.; Kuhne, A.; Bode, W.; Huber, R.; von der Saal, W. et al. X-ray structure of active site-inhibited clotting factor Xa. Implications for drug design and substrate recognition. *J. Biol. Chem.* **1996**, *271*, 29988–29992.
- (65) Guertin, K. R.; Gardner, C. J.; Klein, S. I.; Zulli, A. L.; Czekaj, M.; et al. Optimization of the beta-aminoester class of factor Xa inhibitors. Part 2: Identification of FXV673 as a potent and selective inhibitor with excellent *In vivo* anticoagulant activity. *Bioorg. Med. Chem. Lett.* **2002**, *12*, 1671–1674.
- (66) Arnaiz, D. O.; Zhao, Z.; Liang, A.; Trinh, L.; Witlow, M. et al. Design, synthesis, and *in vitro* biological activity of indole-based factor Xa inhibitors. *Bioorg. Med. Chem. Lett.* **2000**, *10*, 957–961.
- (67) Dudley, D. A.; Bunker, A. M.; Chi, L.; Cody, W. L.; Holland, D. R.; et al. Rational design, synthesis, and biological activity of benzoxazinones as novel factor Xa inhibitors. *J. Med. Chem.* **2000**, *43*, 4063–4070.
- (68) Wiley, M. R.; Weir, L. C.; Briggs, S.; Bryan, N. A.; Buben, J.; et al. Structure-based design of potent, amidine-derived inhibitors of factor Xa: evaluation of selectivity, anticoagulant activity, and antithrombotic activity. *J. Med. Chem.* **2000**, *43*, 883–899.
- (69) Pinto, D. J.; Orwat, M. J.; Wang, S.; Fevig, J. M.; Quan, M. L. et al. Discovery of 1-[3-(aminomethyl)phenyl]-N-3-fluoro-2'-(methylsulfonyl)-[1,1'-biphenyl]-4-yl]-3-(trifluoromethyl)-1H-pyrazole-5-carboxamide (DPC423), a highly potent, selective, and orally bioavailable inhibitor of blood coagulation factor Xa. *J. Med. Chem.* **2001**, *44*, 566–578.
- (70) Nishida, H.; Miyazaki, Y.; Mukaihira, T.; Saitoh, F.; Fukui, M.; et al. Synthesis and evaluation of 1-arylsulfonyl-3-piperazinone derivatives as a factor Xa inhibitor II. Substituent effect on biological activities. *Chem. Pharm. Bull. (Tokyo)* **2002**, *50*, 1187–1194.
- (71) Ewing, W. R.; Becker, M. R.; Manetta, V. E.; Davis, R. S.; Pauls, H. W.; et al. Design and structure-activity relationships of potent and selective inhibitors of blood coagulation factor Xa. *J. Med. Chem.* **1999**, *42*, 3557–3571.
- (72) Quan, M. L.; Ellis, C. D.; Liauw, A. Y.; Alexander, R. S.; Knabb, R. M.; et al. Design and synthesis of isoxazoline derivatives as factor Xa inhibitors. 2. *J. Med. Chem.* **1999**, *42*, 2760–2773.

JM030137A